PHYSICAL REVIEW A **67**, 040701(R) (2003)

Cold collisions of spin-polarized metastable hydrogen atoms

R. C. Forrey,[1] S. Jonsell,[2] A. Saenz,[3] P. Froelich,[4] and A. Dalgarno[5]
[1]*Pennsylvania State University, Berks-Lehigh Valley College, Reading, Pennsylvania 19610-6009*
[2]*Department of Physics, Umeå University, SE-90187 Umeå, Sweden*
[3]*Fachbereich Chemie, Universität Konstanz, Fach M 721, D-78457 Konstanz, Germany*
[4]*Department of Quantum Chemistry, Uppsala University, Box 518, 75120 Uppsala, Sweden*
[5]*Harvard-Smithsonian Center for Astrophysics, 60 Garden Street, Cambridge, Massachusetts 02138*
(Received 23 January 2003; published 10 April 2003)

Cross sections and rate coefficients for collisions of two spin-polarized metastable hydrogen atoms are calculated at low energies and temperatures using complex scaling and Feshbach projection methods for the determination of the molecular potential-energy curves. The inclusion of the Lamb shift and fine-structure splitting of the excited $n=2$ atoms leads to an attractive van der Waals potential for two $2s_{1/2}$ atoms with an exceptionally large coefficient. The quenching of the metastable atoms is dominated at temperatures below 20 mK by ionization. The calculated values for the total loss rate coefficient at 87 μK and 230 μK are within a factor of 2 or 3 of the error bars of recent measurements of metastable loss rate coefficients.

DOI: 10.1103/PhysRevA.67.040701 PACS number(s): 34.10.+x, 03.75.Hh

Bose-Einstein condensation in a gas of spin-polarized hydrogen atoms was achieved in 1998 [1]. In this experiment, two-photon spectroscopy of the $1s$-$2s$ transition was used to determine the temperature and density of the condensate through studies of the collisionally shifted and broadened spectral lines [2,3]. Recent improvements in the apparatus at MIT have allowed more than 10^7 metastable $2s$ atoms to be produced at densities greater than 10^{10} cm^{-3} and temperatures ranging from 300 mK down to 20 μK [4]. These trapped metastable clouds have led to new experiments [4] on the decay of $2s$ hydrogen atoms. Hydrogen is an ideal system for studying fundamental physics and a detailed understanding of the collisional behavior is an important step towards achieving the goal of high-resolution metastable hydrogen spectroscopy.

Collisional quenching may occur from ionization or excitation transfer. Ionization may proceed through the associative reaction

$$\mathrm{H}(2s)+\mathrm{H}(2s)\rightarrow \mathrm{H}_2^+ + e^-, \tag{1}$$

which releases between 6.8 eV and 9.5 eV depending on the final state of the molecular ion, and through the dissociative Penning process

$$\mathrm{H}(2s)+\mathrm{H}(2s)\rightarrow \mathrm{H}(1s)+\mathrm{H}^+ + e^-, \tag{2}$$

which releases 6.8 eV of kinetic energy. In both of these reactions, the ion and electron products would immediately fly out of the magnetic trap [4]. Measurements have been reported [5] for cross sections of associative ionization of metastable hydrogen atoms at energies as low as 48 K. At this temperature, we calculated that the total ionization cross section is 100 times larger than the experimental result, indicating that Penning ionization is the dominant ionization channel. However, theoretical studies [6] suggested that the collisional quenching proceeds preferentially via the double excitation transfer reaction

$$\mathrm{H}(2s)+\mathrm{H}(2s)\rightarrow \mathrm{H}(2p)+\mathrm{H}(2p), \tag{3}$$

a conclusion that may be modified at lower temperatures when the Lamb shift and fine-structure splittings are taken into account in the dynamics.

The principal mechanism by which excitation transfer occurs is the accumulation of differences in phase in the scattering on multiple interaction potentials, which is expected to dominate over the contribution from the weak Coriolis force. The spin-polarized $2s_{1/2}$ atoms approach each other in a $^3\Sigma_u^+$ molecular state of H_2 with total angular-momentum projection quantum number $\Omega=\Lambda+\Sigma=1$. Consistent with the neglect of the Coriolis interaction, we restrict the basis set describing the scattering to molecular states with $\Omega=1$, separating into products of atoms with principal quantum number $n=2$. Asymptotically, the molecular Born-Oppenheimer wave functions tend to linear combinations of the product of atom wave functions $|n,l,m\rangle_a|n',l',m'\rangle_b$ with $n=2$ on nuclei a and b, where l and m are the angular-momentum orbital and projection quantum numbers, respectively. There are nine symmetrized wave functions separating into mixtures of the products

$$\phi_1=|2,0,0\rangle_a|2,0,0\rangle_b\chi_{11}, \tag{4}$$

$$\phi_2=|2,1,0\rangle_a|2,1,0\rangle_b\chi_{11}, \tag{5}$$

$$\phi_3=\frac{1}{\sqrt{2}}[|2,0,0\rangle_a|2,1,0\rangle_b-|2,1,0\rangle_a|2,0,0\rangle_b]\chi_{11}, \tag{6}$$

$$\phi_4=\frac{1}{\sqrt{2}}[|2,1,1\rangle_a|2,1,-1\rangle_b+|2,1,-1\rangle_a|2,1,1\rangle_b]\chi_{11}, \tag{7}$$

$$\phi_5=\frac{1}{\sqrt{2}}[|2,1,0\rangle_a|2,1,1\rangle_b+|2,1,1\rangle_a|2,1,0\rangle_b]\chi_{10}, \tag{8}$$

$$\phi_6=\frac{1}{\sqrt{2}}[|2,1,0\rangle_a|2,1,1\rangle_b-|2,1,1\rangle_a|2,1,0\rangle_b]\chi_{00}, \tag{9}$$

$$\phi_7 = |2,1,1\rangle_a |2,1,1\rangle_b \chi_{1-1}, \tag{10}$$

$$\phi_8 = \frac{1}{\sqrt{2}}[|2,0,0\rangle_a |2,1,1\rangle_b + |2,1,1\rangle_a |2,0,0\rangle_b]\chi_{10}, \tag{11}$$

$$\phi_9 = \frac{1}{\sqrt{2}}[|2,0,0\rangle_a |2,1,1\rangle_b - |2,1,1\rangle_a |2,0,0\rangle_b]\chi_{00}, \tag{12}$$

where $\chi_{S\Sigma}$ is the molecular electronic spin wave function. The matrix of the electrostatic interaction is a diagonal matrix with nine elements $V_i(\boldsymbol{R})$ equal to the Born-Oppenheimer interaction potentials, with R being the internuclear distance. The potentials are complex functions of R. The imaginary parts permit ionization to occur [6]. Degenerate perturbation theory must be used to determine the form at large R of the real parts of the interaction potentials V_1, V_2, and V_4 corresponding to mixtures of the $^3\Sigma_u^+$ states ϕ_1, ϕ_2, and ϕ_4. We find for the nine states

$$V_1 = -9\sqrt{6}R^{-3} + 648R^{-5} + O(R^{-6}), \tag{13}$$

$$V_2 = O(R^{-6}), \tag{14}$$

$$V_3 = 18R^{-3} + O(R^{-6}), \tag{15}$$

$$V_4 = 9\sqrt{6}R^{-3} + 648R^{-5} + O(R^{-6}), \tag{16}$$

$$V_5 = -864R^{-5} + O(R^{-6}), \tag{17}$$

$$V_6 = O(R^{-6}), \tag{18}$$

$$V_7 = 216R^{-5} + O(R^{-6}), \tag{19}$$

$$V_8 = -9R^{-3} + O(R^{-6}), \tag{20}$$

$$V_9 = 9R^{-3} + O(R^{-6}). \tag{21}$$

The potentials V_1, V_2, V_3, and V_4 correspond to molecular states of $^3\Sigma_u^+$ symmetry. They have been obtained previously by use of the complex scaling method [7]. We have extended the calculations to the other five states using a Feshbach projection technique [8]. The potentials V_5, V_6, and V_7 correspond to $^3\Pi_u$, $^1\Pi_u$, and $^3\Delta_u$ states, respectively, and V_8 and V_9 correspond to $^3\Pi_u$ and $^1\Pi_u$ states, respectively. The potentials V_3, V_8, and V_9 do not enter the scattering calculations [9] and single excitation transfer is expected to be inefficient. The results of the complex scaling and Feshbach projection calculations agree closely with the asymptotic forms (13)–(21) given by the first-order perturbation theory, allowing a smooth matching procedure to be performed.

The energy-level degeneracy is lifted by the fine-structure splitting and the Lamb shift. In order to include these effects, we transform from LS to jj coupling and introduce the $\Psi(j,\Omega,l_a,l_b,j_a,j_b)$ representation, where $\vec{j} = \vec{j}_a + \vec{j}_b$, and $\Omega = m_{j_a} + m_{j_b}$, and construct the symmetry adapted basis functions

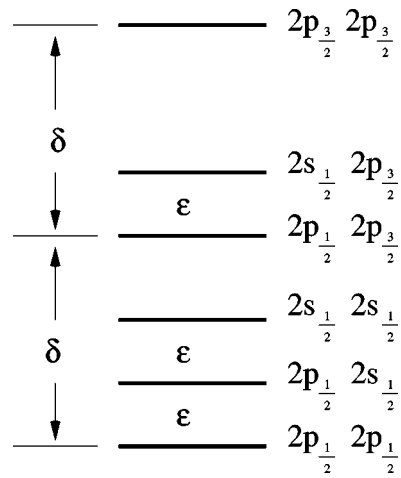

FIG. 1. Energy-level diagram for product $n=2$ hydrogen atoms. The Lamb shift and fine-structure splittings are $\epsilon = 1.61\times10^{-7}$ a.u. and $\delta = 1.67\times10^{-6}$ a.u., respectively.

$$\psi_1 = \Psi(1,1,0,0,\tfrac{1}{2},\tfrac{1}{2}), \tag{22}$$

$$\psi_2 = \Psi(1,1,1,1,\tfrac{1}{2},\tfrac{1}{2}), \tag{23}$$

$$\psi_3 = \frac{1}{\sqrt{2}}[\Psi(1,1,1,1,\tfrac{1}{2},\tfrac{3}{2}) - \Psi(1,1,1,1,\tfrac{3}{2},\tfrac{1}{2})], \tag{24}$$

$$\psi_4 = \Psi(1,1,1,1,\tfrac{3}{2},\tfrac{3}{2}), \tag{25}$$

$$\psi_5 = \frac{1}{\sqrt{2}}[\Psi(2,1,1,1,\tfrac{1}{2},\tfrac{3}{2}) + \Psi(2,1,1,1,\tfrac{3}{2},\tfrac{1}{2})], \tag{26}$$

$$\psi_6 = \Psi(3,1,1,1,\tfrac{3}{2},\tfrac{3}{2}). \tag{27}$$

This procedure adds the energy defects along the diagonal of the interaction matrix $V_{ij}(R)$ and introduces couplings between the eigenstates that are neglected in the nonrelativistic approximation. A new set of adiabatic potentials is obtained by diagonalizing the matrix $V_{ij}(\boldsymbol{R})$ as a function of $\boldsymbol{R}$. Figure 1 illustrates the energy-level structure of pairs of $\boldsymbol{n}=2$ states of hydrogen. The Lamb shift and fine-structure defects are $\epsilon = 1.61\times10^{-7}$ a.u., and $\delta = 1.67\times10^{-6}$ a.u., respectively. Figure 2 shows the real parts of the new adiabatic potentials. The dashed curves are the Born-Oppenheimer potentials V_1, V_2, and V_4. The lowest solid curve corresponds to a pair of $2p_{1/2}$ atoms. The spin-polarized metastable hydrogen atoms approach along the second lowest solid curve. If we set the zero of the energy scale at the $2p_{1/2}$,$2p_{1/2}$ limit, then the $2s$,$2s$ energy lies at 2ϵ. The long-range $2s_{1/2}$-$2s_{1/2}$ interaction is a van der Waals attraction varying as R^{-6} with an exceptionally large coefficient $C_6 = -18\epsilon^{-1} + 252(\delta - 2\epsilon)^{-1} + 99(\delta - \epsilon)^{-1} \approx 1.4\times10^8$ a.u. Figure 3 shows an enlargement of the long-range interaction for several values of nuclear orbital angular-momentum quantum number l. The long-range interaction exerts a strong influence on the scattering at energies near to the heights of the centrifugal barriers.

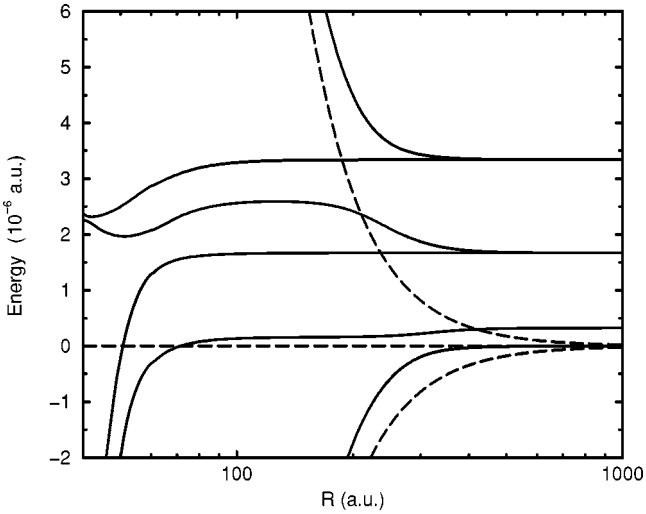

FIG. 2. Adiabatic potential curves (solid lines) obtained by diagonalizing $V_{ij}(R)$ as a function of R. The curves separate asymptotically into the pairs $(2p_{1/2},2p_{1/2})$, $(2s_{1/2},2s_{1/2})$, $(2p_{1/2},2p_{3/2})$, and $(2p_{3/2},2p_{3/2})$. The dashed curves are the Born-Oppenheimer potentials V_1, V_2, and V_4 [see Eqs. (13), (14), and (16)].

The diabatic scattering formulation with potential coupling matrix $V_{ij}(R)$ obtained in the ψ_q representation (22)–(27) was used to compute the cross sections. When the nuclear symmetry is included along with the electronic symmetry, the cross sections are given by

$$\sigma_{pq}=\frac{\pi}{2k_p^2}\sum_{l=0}^{\infty}(2l+1)[1+(-1)^l]^2|S_{pq}^{(l)}-\delta_{pq}|^2, \quad (28)$$

$$\sigma_p^{\text{ion}}=\frac{\pi}{2k_p^2}\sum_{l=0}^{\infty}(2l+1)[1+(-1)^l]^2\left[1-\sum_q |S_{pq}^{(l)}|^2\right], \quad (29)$$

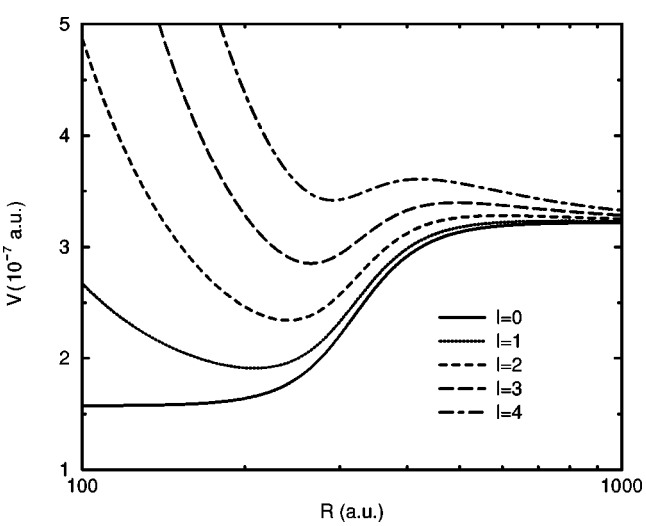

FIG. 3. Adiabatic potential curves for the lth partial wave for the state that separates asymptotically to two $2s_{1/2}$ atoms. The potential well has a strong effect on the dynamics of energies near the centrifugal barrier.

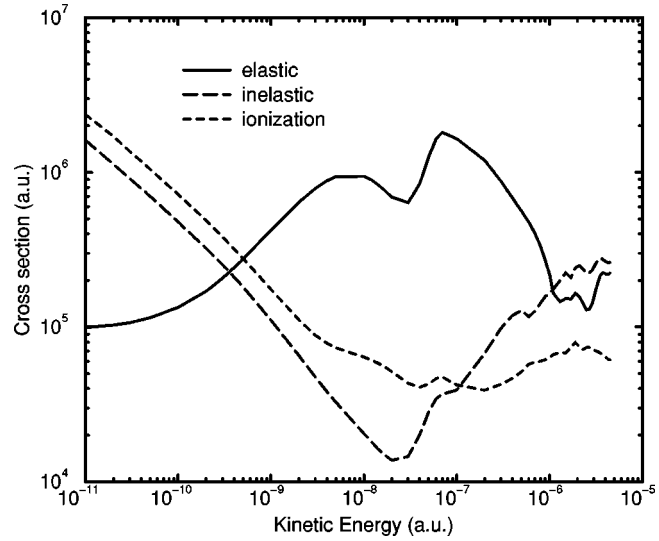

FIG. 4. Cross sections for elastic scattering (solid curve), inelastic double excitation transfer (long dashed curve), and ionization (short dashed curve).

where $q=1,\ldots,6$, $p=1$ is the entrance channel, and $S_{pq}^{(l)}$ is the element of the scattering matrix for the lth partial wave. Our scattering calculations use a multichannel Numerov propagation with a complex interaction potential. The coupling matrix V_{ij} was tested by computing the cross sections (28) and (29) with the energy defects set to zero. With zero energy defects, the simple method of Ref. [6] can be applied. The calculations in Ref. [6] are based on the singlet states of H_2. For the triplet states, the same method yields the elastic, inelastic, and ionization cross sections $4600E^{-1/2}$ a.u., $4400E^{-1/2}$ a.u., and $15E^{-2/3}$ a.u., respectively, which are identical to those we find here by solving the diabatic scat-

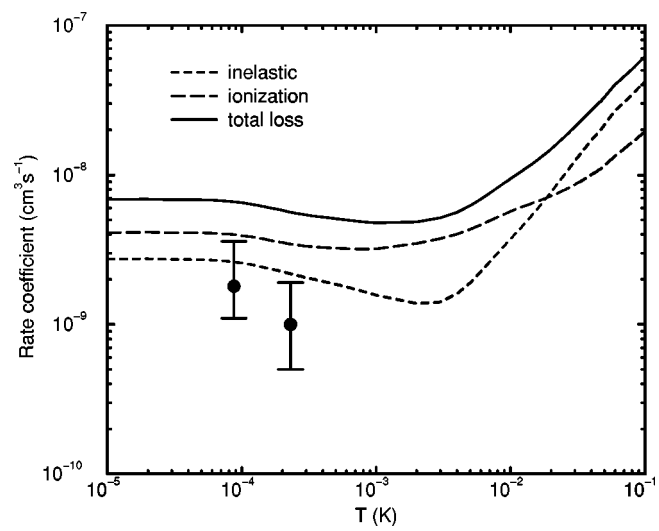

FIG. 5. Loss rate coefficients for inelastic double excitation transfer (dashed curve), ionization (long dashed curve), and the theoretical (solid curve) and experimental [4] values of the total loss rate coefficient. The theoretical values have been thermally averaged and multiplied by two in order to account for the loss of two metastable particles per collision.

tering equations with $\epsilon = \delta = 0$. The cross sections obtained when the energy defects are included in the interaction matrix are shown in Fig. 4. The oscillation in the elastic cross section is a consequence of the long-range attraction of the adiabatic potential. The potential wells shown in Fig. 3 support shape resonances in the cross section at energies comparable to the barrier heights. Due to symmetry, the contribution from the $l = 3$ partial wave is missing from Eq. (28). The elastic cross section shows a minimum at the position of the missing $l = 3$ resonance and a strong upturn at the position of the $l = 4$ resonance. In the ultracold limit, the system may be described by the complex scattering length $(33 - 22i) \times 10^{-8}$ cm.

Figure 5 shows the loss rate coefficients for scattering and ionization, and the theoretical and experimental values [4] of the total loss rate coefficient. The theoretical values have been thermally averaged and multiplied by 2 in order to account for the loss of two metastable particles per collision. The theoretical values are within a factor of 2 or 3 of the experimental error bars. Refinements in the theory are in progress. The influence of the nonadiabatic radial and angular-momentum coupling terms will yield some contribution to the quenching from single excitation transfer, and the hyperfine interaction may produce small corrections to the calculated rate coefficients.

Helpful conversations with D. Landhuis are gratefully acknowledged. The research has been variously supported by the National Science Foundation through grants to the Center for Ultracold Atoms, the Institute for Theoretical Atomic and Molecular Physics, and Grant No. PHY-0070920 to R.C.F. A.D. acknowledges support by the Chemical Sciences, Geosciences and Biosciences Division of the Office of Basic Energy Sciences, U.S. Department of Energy. S.J. and P.F. acknowledge support by the Swedish Research Council and A.S. acknowledges support by the Deutsche Forschungsgemeinschaft (DFG) in the framework of SPP 1116.

[1] D.G. Fried, T.C. Killian, L. Willmann, D. Landhuis, S.C. Moss, D. Kleppner, and T.J. Greytak, Phys. Rev. Lett. **81**, 3811 (1998).

[2] C.L. Cesar, D.G. Fried, T.C. Killian, A.D. Polcyn, J.C. Sandberg, I.A. Yu, T.J. Greytak, D. Kleppner, and J.M. Doyle, Phys. Rev. Lett. **77**, 255 (1996).

[3] T.C. Killian, D.G. Fried, L. Willmann, D. Landhuis, S.C. Moss, T.J. Greytak, and D. Kleppner, Phys. Rev. Lett. **81**, 3807 (1998).

[4] D. Landhuis, L. Matos, S. C. Moss, J. K. Steinberger, K. Vant, L. Willmann, T. J. Greytak, and D. Kleppner, Phys. Rev. A **67**, 022718 (2003); D. Landhuis, Ph.D. thesis, Harvard University, 2002 (unpublished).

[5] X. Urbain, A. Cornet, and J. Jureta, J. Phys. B **25**, L189 (1992).

[6] R.C. Forrey, R. Cote, A. Dalgarno, S. Jonsell, A. Saenz, and P. Froelich, Phys. Rev. Lett. **85**, 4245 (2000).

[7] S. Jonsell, A. Saenz, P. Froelich, R.C. Forrey, R. Cote, and A. Dalgarno, Phys. Rev. A **65**, 042501 (2002).

[8] A. Saenz *et al.* (unpublished).

[9] S.I. Nikitin, V.N. Ostrovskii, and N.V. Prodov, Sov. Phys. JETP **64**, 745 (1986).